UNIVERSITY of CALIFORNIA
SANTA CRUZ

SPECTROSCOPIC GALAXY CLUSTER OBSERVATIONS FOR THE DARK ENERGY SURVEY

A thesis submitted in partial satisfaction of the
requirements for the degree of

BACHELOR OF SCIENCE

in

PHYSICS (ASTROPHYSICS)

by

Benjamin E. Stahl

August 2015

The thesis of Benjamin E. Stahl is approved by:

Professor Tesla Jeltema Advisor	Adriane Steinacker Theses Coordinator

Professor Robert Johnson
Chair, Department of Physics

Abstract

Spectroscopic Galaxy Cluster Observations for the Dark Energy Survey

by

Benjamin E. Stahl

The DEIMOS instrument on Keck II was used for 2.5 nights during the fourth quarter of 2014 to obtain high-resolution multi-slit spectroscopic measurements on two Dark Energy Survey (DES) targeted galaxy clusters. The observations were reduced using a slightly modified version of the Spec2d Data Reduction Pipeline and then the science-ready outputs were analyzed using a tool called SpecPro. Specifically, SpecPro was used to determine the redshifts of all the observed galaxies thereby allowing for a catalog of redshifts to be created. The redshifts of the two observed DES clusters were determined to be 1.049 ± 0.005 and 0.955 ± 0.003, while the velocity dispersions were found to be 680 km s^{-1} and 510 km s^{-1}, respectively. Cluster masses were determined to be 3.7×10^{14} $M_{\odot}$ and 1.7×10^{14} $M_{\odot}$. The clusters were chosen specifically because of Keck's ability to observe them depsite their high redshift. The catalog of redshifts will complement the work of other DES groups who have observed lower redshift clusters. Ultimately, the combined catalog of redshifts will aid DES in constraining and calibrating their results.

Contents

List of Figures

List of Tables

Acknowledgements

The project presented in this paper would not have been possible without the mentorship, encouragement, and support of the following people and organizations:

I would like to thank my advisor, Professor Tesla Jeltema, for mentoring me and including me in her research activities. She helped to define this project for me and really gave me the freedom to learn and develop my research skills. I am also grateful to her for bringing me along to Keck in Hawaii for the data collection, and for giving such timely and useful feedback on the drafts of this thesis. I would like to thank Devon Hollowood for assisting in the observations and for helping me sort through code and computer issues as they arose in my work. Dr Bradford Holden also spent many hours meeting with me to help address problems arising during the reduction of the data. Special thanks go to Michael Cooper who illuminated and shared the solution to the problem of incorrect wavelength solutions during data reduction.

This project was supported by funds from the National Science Foundation, the Department of Energy, and the UCSC Undergraduate Research in Sciences Award.

1

Introduction

Current cosmological observations suggest that there is an energy associated with otherwise empty space on all length scales. Without this 'Dark Energy', cosmological theories cannot successfully explain why the Universe is flat, nor can they explain a host of bizarre effects that are readily observed such as the fact that the Universe is not only expanding, but accelerating in its expansion [5]. Alternative explanations have been proposed to account for these effects, such as the assertion that general relativity may not be accurate on scales larger than superclusters of galaxies. However, it is broadly held that new physics - the Dark Energy - will be required to fully explain the observations.

One proposed form for Dark Energy is a scalar field such as quintessence, which is a dynamic quantity whose energy density need not be constant in space and time. A simpler solution is a cosmological constant (Λ); this leads to the Lambda Cold Dark Matter (ΛCDM) model, which is currently the most utilized cosmological theory. The cosmological constant is the energy density of the vacuum (i.e. empty space) and is uniform throughout space. The idea was first introduced in 1917 by Einstein to counteract the effects of gravity and make the Universe static. However, in 1929 Edwin Hubble discovered that all galaxies outside of the Local group are moving away from one another, thus suggesting that the Universe is expanding as a whole [4]. Common scientific lore claims that Einstein thought of his

cosmological constant as his biggest mistake. Hubble's discovery led to a paradigm lasting until the 1990's that assumed the cosmological constant was zero. In 1998 however, observations of the relation between distance and redshift (z) for Type Ia supernovae were published showing that the expansion of the Universe is accelerating [8] [10]. Since these astonishing results were published, evidence for this 'cosmic acceleration' has been found in measurements of the cosmic microwave background by the WMAP and Planck satellites, as well as from a host of other sources.

ΛCDM successfully explains these observations and also predicts that Dark Energy is very homogeneous and extremely low density ($\sim 10^{-30}$ g/cm^3 on mass-energy equivalence basis) [2]. With such a low density, Dark Energy is likely undetectable in a standard laboratory experiment and is also not expected to interact with any of the fundamental forces of nature except for gravity. Dark Energy has an enormous effect on the Universe only because it uniformly fills all of space. Current results suggest that Dark Energy accounts for 68.3% of the mass-energy density of the Universe, that Dark Matter accounts for 26.8%, and that the remaining 4.9% is in ordinary baryonic matter [9].

On the forefront of current observational studies into Dark Energy is an international collaboration known as the Dark Energy Survey (DES). Photometric data collection of a 5000 deg^2 patch of the Southern sky was commenced by DES in September 2013 as part of a 5 year mission that aims to study the nature of Dark Energy in unprecedented quantitative detail [12]. DES will use the following four methods to study the nature of Dark Energy:

- Counting galaxy clusters and measuring their spatial distribution at $0 < z < 1$.
- Weak lensing on redshift shells up to $z \sim 1$.
- Baryon acoustic oscillations.
- Type Ia supernovae at $0.3 < z < 0.8$.

Clearly, redshift plays an important role in the methods of the survey and will be funda-

mental to some of the studies. Redshift is so integral because it encodes a vast amount of information about an object including notions of age, distance, velocity, and so on. Given the relevance, photometric redshifts will be included in DES data products. Such redshifts, which are calculated from the flux in a handful of photometric filters, are inherently imprecise compared to those that are calculated from spectroscopic observations. However, the technique of photometric redshifts is much more efficient in terms of telescope time, and is suited to the vast number of observations that DES is making.

Most of the scientific goals of DES will not be hindered by the lower precision, but a dominant source of systematic error in their galaxy cluster program of study will be the determination of the mass of a cluster [12]. As such there is a need to probe and quantify the systematic errors as well as calibrate a mass-observable relation. For DES this observable is cluster richness, which is essentially a measure of the number of member galaxies in a cluster. In order to calibrate the richness-mass relation, two DES galaxy clusters were selected for follow up spectroscopic observations that will allow for the redshift of member galaxies and subsequently through dynamics, the mass of each observed cluster to be determined to a high level of precision. These clusters were chosen specifically for observation on Keck because their high redshifts ($z \sim 1$) make them difficult to observe with other telescopes. The spectroscopic redshift determinations discussed in this paper will be added to larger samples of lower redshift clusters that have been observed by other DES groups, which will ultimately allow DES to constain and calibrate their photometric redshifts.

These follow up spectroscopic observations and the related analysis form the basis of the scientific project detailed in this paper. High resolution spectroscopic measurements of galaxies within two DES clusters were made at the W.M. Keck Observatory. These observations were then used to determine the redshift and mass of the clusters. This was accomplished by completing a series of objectives leading from experimental design, to observation, to data reduction, to analysis, and ultimately to a conclusion.

2

Observations

2.1 Experimental Apparatus

Experimental data was taken using the following instruments and equipment:

Telescope: Keck II 10 m reflecting telescope located at the summit of Mauna Kea, Hawaii.

Detector: Deep Imaging Multi-Object Spectrograph (DEIMOS) [15].

- 8k x 8k detector mosaic utilizing eight MIT/Lincoln Labs CCDs[1].
- Located at Nasmyth focus of Keck II
- Slitmasks[2]: 0223_1, 0223_2, DES215B, DES215_B, & DES215_3
- Grating: 1200G (1200 lines/mm)
- Filter: OG550

2.2 Calibration & Set Up

A total of three observing sessions were completed using the experimental apparatus described in Section 2.1. The first session was conducted remotely from the UCSC remote observations room in the basement of the Natural Sciences building during the second half

[1] Each of the CCDs is 2k x 4k.

[2] Cluster DES0223-0416 was observed with 0223_1 & 0223_2, DES0215-0458 was observed with the others.

of the night of September 21, 2014. The remaining two sessions were conducted from the W.M. Keck Observatory control room in Waimea, Hawaii on back-to-back full nights starting on October 23, 2014. For each observing session regardless of where the observations were conducted, the set up and calibration procedures in the DEIMOS manual were followed and will be briefly outlined now[3] [14].

First the remote desktop software that allows for the instrument to be manipulated and controlled was started and then the status of DEIMOS was checked. Once reporting ready, it was started up and then it was verified that the correct slitmasks, gratings, and filters were in place for the observing run. Next, a test exposure was taken and then a series of tasks were completed to align the slitmasks to be used during the observing session. Then a series of exposures were taken to focus the instrument. The flexure compensation system (FCS) was calibrated. Finally, calibration exposures were taken to later allow for instrumental bias to be removed from the data. These included internal flat field and arc lamp[4] exposures. Upon completion of these exposures and all of the other intricacies in the DEIMOS manual, the apparatus was considered ready for scientific data collection.

2.3 Science Data Collection

After completing the calibration and set up procedures as prescribed in Section 2.2 prior to each session of observation, scientific data collection was commenced. The telescope was pointed to the coordinates of the target, guiding was enabled, and then a sequence of 30 minute exposures were taken. On the half night, slitmask '0223_2' was used with six science exposures, then on the first full night (October 23, 2014), slitmasks '0223_1' (6 science exposures) and 'DES215B' (7 science exposures) were used for observing. During the final session on the following night, the 'DES215_B' (6 science exposures) and 'DES215_3' (7 science exposures) masks were used for observation.

[3]It should be noted that the observer using the instrument for the first half of the night preceding the first observing session conducted these procures, while the author and collaborators of this paper conducted the procedures on both of the full night observing sessions.

[4]The arc lamp exposures were taken with the following arc lamps activated: Kr, Xe, Ar, & Ne.

3

Data

Having successfully completed 3 observing sessions in which 5 slit masks were used in the collection of spectroscopic measurements of the galaxies within two galaxy clusters targeted by DES, the process of reducing the raw data was then commenced. The process by which this data reduction, which converted the raw multi-slit spectral images into science ready data products, was accomplished will be detailed in the following sections.

3.1 Spec2d Data Reduction Pipeline

The bulk of the data reduction process was accomplished using an existing suite of IDL routines known as the Spec2d Data Reduction Pipeline [3] [7]. This pipeline was developed for the DEEP2 Galaxy Redshift Survey, which used $\sim$ 90 nights of observing time on DEIMOS to collect over 50,000 spectra of galaxies at $z \sim 1$. Given that the pipeline was designed for reducing two-dimensional spectra taken with DEIMOS (and specifically the 1200 line/mm grating) of galaxies at comparable redshifts to those that were observed for this paper, the Spec2d pipeline was a natural choice for data reduction. The process by which the pipeline was used to reduce the raw two-dimensional spectra that were obtained during the observing sessions will be detailed in the following subsections.

3.1.1 Spec2d Version and Modifications

Changes to the DEIMOS instrument over the years have made the original pipeline employed by the DEEP2 team prone to failures. Specifically, a failure mode in which an incorrect wavelength solution is obtained was experienced during the reduction of the observations presented in this paper. To rectify the problem, the beta version of the pipline was used with some slight modifications to the code, which are detailed in Appendix A.

3.1.2 Plan File

The first step in using the Spec2d data reduction pipeline is to create a plain-text file (with the extension `.plan`) containing keywords and values that specify how and what data to reduce. Creating the 'plan file', as it is called, can be completed in an automated fashion by running the IDL routine `deimos_planfile.pro` from an IDL session initiated in the same directory as the raw data to be reduced. This automated method creates a plan file that specifies the flat field frames, arc frames, and science frames associated with a given mask as well as the mask and raw data directory. It also specifies the 'poly' wavelength fitting scheme by default. The plan files that were used to reduce the collected data were generated using this automated routine and then modified to select only specific CCDs (chips) to perform the reduction on using the 'CHIPS' keyword. Given the configuration of the CCD array (Figure 3.1) and the shape of the observed clusters, a given slitmask did not necessarily have slits cut that would allow light to fall on all of the chips.

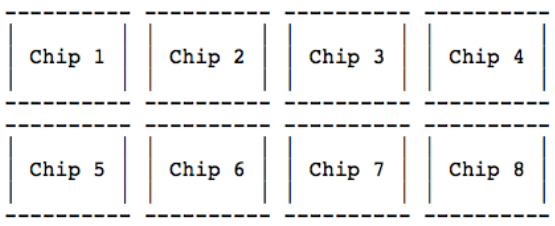

Figure 3.1: Numbering scheme for the chips in the DEIMOS CCD array as used by the Spec2d Data Reduction Pipeline [13].

Thus, the chips that had no light fall upon them were excluded from the reduction. Further,

due to challenges with the data reduction pipeline there were several additional chips that were not reduced. Table 3.1 shows which chips were reduced for each mask:

Mask	Chips
0223_1	3,7
0223_2	2,3,6,7
DES215B	2,6
DES215_B	2,6
DES215_3	2,3,6,7

Table 3.1: The CCD chips that were reduced for each slitmask.

Having created plan files[1] for each slit mask with the desired chips specified following the process detailed above, the observations were then run through the pipeline. This was done by using a master program called `domask.pro` in a 32-bit IDL session that draws the information from a specified plan file and then manages the data reduction process.

3.1.3 Reduction Process

The method of data reduction performed by the Spec2d Data Reduction Pipeline is extensively detailed by Newman et al. (2013) but will be outlined now in the fashion that it was used for the observations reported in this paper [7]. Note that in every step, each CCD is treated separately.

1. **calibSlit:** The specified flat field frames are read in and processed to correct for pixel-to-pixel response variations and reject cosmic rays. Then the slitlets are identified and located. Next, the combined flat field frame for each chip is mapped into rectangular arrays corresponding to each slitlet, effectively creating individual, rectangular flat fields for each slitlet.

2. **Pixel-to-Wavelength Solution:** The arc frame(s) are read in and corrected for pixel-to-pixel response variations. Next, a shift in the spatial direction between the arc data and the original flat field is found using a cross correlation process. After this, arc spectra for each slitlet are extracted and mapped into rectangular arrays

[1] A sample plan file is included in Appendix B.

following the same methods as for the flat field frames. Figure 3.2 shows an example of the arc spectra mapped to slitlets.

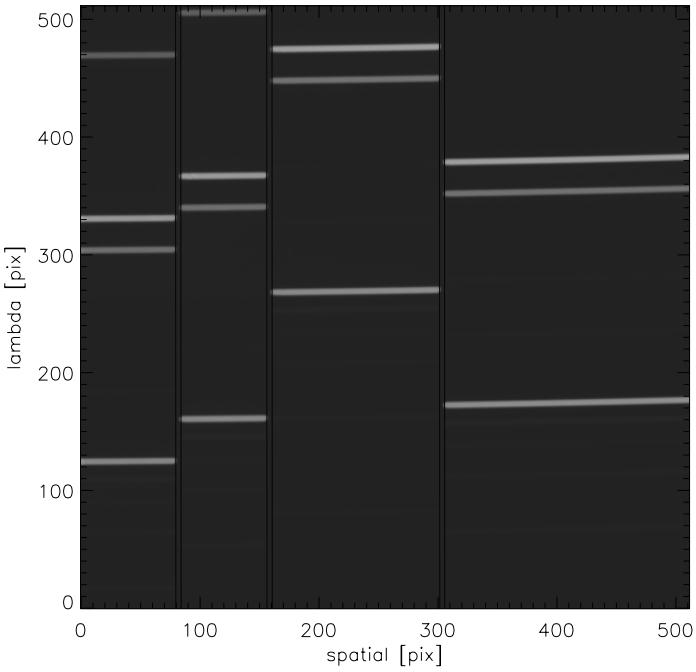

Figure 3.2: Arc lamp spectra mapped to four rectangular arrays corresponding to slitlets in the slitmask '0223_2'.

After constructing the rectangular arc array for each slitlet, a mapping is found between pixel and wavelength space. This process starts with a rough initial guess provided by the DEIMOS optical model[2], and then uses a linear regression process to determine the coefficients of Legendre polynomials up to fifth order that best fit the wavelength as a function of pixel number along the central row of the slitlet. After some further intricacies, the results are written to the `calibSlit` files. At this point these files contain all of the needed information to calibrate each slitlet.

3. **Science Data Rectification:** The science frames are read in and corrected for pixel-to-pixel response variations, then the slitlets are extracted and converted to rectangular arrays following the same process as for the other frames. Flat field corrections are then applied to each slitlet. From photon and read noise, an inverse-

[2]This optical model is what is altered and is discussed in Appendix A.

variance image is also produced. Next, a B-spline model is used to fit the sky intensity as a function of wavelength to the sky regions of each slitlet, thus allowing for sky lines to be subtracted in the following step. At the completion of this step, a `spSlit` file is written for each slitlet that contains the reduced 2D spectra from each science frame as well as the other generated attributes.

4. **Science 2D Spectra:** In this step, the science exposures for each slitlet that were generated in the previous step are combined into one inverse-variance weighted mean, sky-subtracted, and cosmic ray rejected two dimensional spectrum. The result for each slitlet is written into a `slit` file along with the wavelength solution and various other information pertaining to the reduction. At this point, the two-dimensional reduction is considered complete.

5. **1D Spectrum Extraction:** In this final step, a one-dimensional science ready spectrum is extracted from the completed and combined two-dimensional spectra produced in the previous step. Multiple extraction methods are available, and the default 'optimal extraction' method was utilized for all of the data being reported in this paper. Each extracted one-dimensional spectrum is written to a `spec1d` file, even if multiple objects fall on the same slitlet. In such cases where a `spSlit` file contains more than one object, the pipeline produces a `spec1d` file for each object, and labels suspected serendipitous objects in the file name.

3.2 Preparation for Analysis

As will be discussed in the following sections, an interactive tool called SpecPro was used to perform significant parts of the analysis such as redshift determination [6]. In order to use this tool, the science ready products from the Spec2d Pipeline, namely the `spec1d` and `slit` files, were converted using the Keck DEIMOS 1D/2D wrapper [1]. For convenience, a Python script was written to automate the process of using the wrapper. This script can be made available by contacting the author.

4

Analysis & Results

Having corrected and calibrated the science frames according to the methodologies described in Section 3, a process of scientific analysis was conducted. The details of this analysis and the results of it will be presented in the following sections.

4.1 Redshift

The first step in the scientific analysis was to calculate the redshift of each galaxy for which a one-dimensional object spectrum was extracted. This was accomplished in a semi-automated fashion that will be detailed in the following section, and then the results from this analysis will be presented in the subsequent section.

4.1.1 Redshift Determination

The redshift of each observed galaxy was determined using an interactive IDL tool called SpecPro. Presentation of the full functionality and methodology of SpecPro are deferred to Masters et al. (2011), but the process by which the software was used to extract redshifts for this paper will be detailed in the following steps. Prior to starting these steps, the data must be in SpecPro format as discussed in Section 3.2.

1. **Start Up:** From a 32-bit IDL session the SpecPro tool is initiated fromt the prompt by typing `specpro, xxx`, where `xxx` denotes the slit number to start on. This will

open the SpecPro utility in a new window, if there are multiple spectra for the same slit (i.e. serendipitous spectra) then a dialog box will open that allows the user to select which spectrum to use.

2. **Configuration:** While SpecPro can read in a total of five[1] files for a given slit, only the one and two dimensional spectra were used for the analysis being reported in this paper. Next, the displayed one-dimensional spectrum was binned and smoothed[2] to better visualize the features in the spectrum. Many additional adjustments are possible, but these were the only ones made at this stage.

3. **Model Fitting:** After obtaining a good visual representation of the features in the spectrum, the redshift is obtained by using SpecPro to run a cross-correlation between a selected spectral template[3]. The six best fitting solutions are available for each model that is fit to the spectrum. In infrequent cases where a reasonable fit could not be obtained with a model, this step was skipped.

4. **Verification & Adjustment:** Once a solution for the redshift was selected from one of the fitted models, a verification was performed by overlaying specific spectral lines on top of the spectrum to verify that there was indeed absorption or emission where it should be. Should the fit not be perfectly aligned, the model was offset along the wavelength axis to line up more precisely with the observed spectrum and thus obtain a more accurate redshift. If no model fitting was used, then the redshift was found by matching known spectral lines to the observed spectrum.

5. **Output:** Although SpecPro does provide for output of the results, this feature was not used because a more thorough accounting of the redshifts and the confidence in them was desired. Thus for each slitlet, the previous three steps were performed (the software need not be restarted for each slitlet) and the results for each slitlet were recorded into a file that contained the results for all the slitlets in a given mask.

[1] 1D spectrum, 2D spectrum, stamp image, photometry, information.

[2] Inverse variance weighted average in the vicinity of each pixel to reduce the noise.

[3] The spectral templates that were used for cross-correlation were: VVDS Elliptical, VVDS S0, VVDS Early Spiral, and VVDS Spiral.

Figure 4.1 shows the SpecPro tool in use and serves to illustrate how it was used to determine the redshift a galaxy.

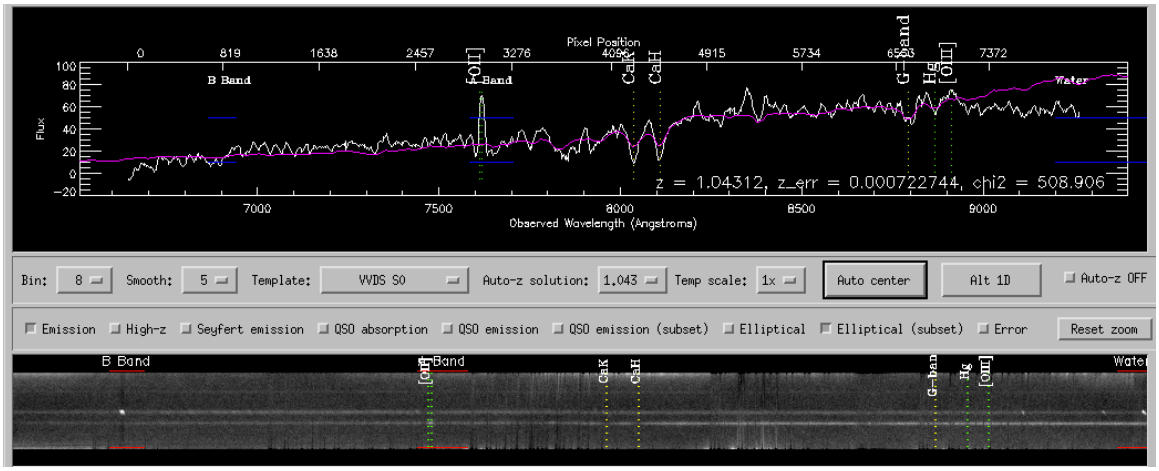

Figure 4.1: Screenshot of the SpecPro tool in use analyzing the spectra of a DES0223-0416 member galaxy. The top graph shows the one-dimensional galaxy spectrum and the bottom shows the two-dimensional spectrum that it was extracted from. Overlayed on the one-dimensional spectrum in magenta is the best fit of the VVDS S0 template, giving the result of $z = 1.043 \pm 0.0007$. Addionally, specific spectral lines such as OII emission and Ca H, Ca K, and G-band absorption are overlayed to verify the fit of the model to the true spectrum. In the two-dimensional spectrum there is an obvious serendipitous spectrum showing several strong emission features in addition to the that of the desired target.

4.1.2 Redshift Results

The redshift results obtained using the process described in Section 4.1.1 will be presented, for each DES cluster, in the following tables which were created using a script[4] that pulled all of the pertinent information together from the results files and the original `.fits` files which contained the RA and DEC of the targets.

RA	DEC	Temp	Spectral Lines	z	σ_z	z (best)	Qual
02:24:03.73	-04:13:39.7	Elliptical	CaK,CaH,Hd,G	1.051	0.0011	1.052	3
02:23:58.20	-04:14:20.9	S0	OII,CaK,CaH,G,OIII	1.043	0.0008	1.044	3
		S0	OII,CaK,CaH,Hd,G	1.043	0.0007	1.043	3
02:24:01.87	-04:13:25.3	Elliptical	CaK,CaH,Hd,G	1.040	0.0007	1.041	3
		S0	CaK,CaH,Hd,G	1.040	0.0014	1.041	3
02:23:59.70	-04:13:22.1	Elliptical	CaK,CaH,Hd,G	1.050	0.0006	1.050	3
02:24:03.84	-04:13:11.8	Elliptical	CaK,CaH,G	1.047	0.0011	1.048	3
02:23:59.90	-04:12:35.3	Elliptical	CaK,CaH,Hd,G	1.057	0.0010	1.057	3

Continued on next page...

[4]This script was also used to format the data for typesetting and is available by contacting the author.

Table 4.1 ...continued from previous page

RA	DEC	Temp	Spectral Lines	z	σ_z	z (best)	Qual
		S0	OII,CaK,CaH,Hd,G	1.057	0.0009	1.057	3
02:24:04.82	-04:13:23.2	none	none	none	none	none	1
02:24:04.18	-04:13:26.5	Elliptical	CaK,CaH,Hd,G	1.051	0.0005	1.051	3
02:24:09.16	-04:14:42.2	Elliptical	CaK,CaH,Hd,G	0.871	0.0005	0.872	3
02:24:03.59	-04:13:05.3	Elliptical	CaK,CaH,Hd,G	1.052	0.0004	1.053	3
02:24:08.22	-04:12:34.7	Elliptical	CaK,CaH,Hd	1.148	0.0010	1.149	3
02:24:04.85	-04:13:33.4	none	none	none	none	none	1
0.0	0.0	none	none	none	none	none	1
0.0	0.0	Early Spiral	OII,Hg,Hb,OIII	0.850	0.0003	0.849	3
0.0	0.0	Early Spiral	OII,Hg	1.040	0.0018	1.039	3
0.0	0.0	Elliptical	CaK,CaH,G	1.052	0.0009	1.052	3
0.0	0.0	none	none	none	none	none	1
0.0	0.0	none	none	none	none	none	1
0.0	0.0	none	none	none	none	none	1

Table 4.1: Redshift results for DES0223-0416. The first and second columns give the RA and DEC of the galaxy, respectively. The next column gives the spectral template that was used to fit the observed spectrum, and the next column identifies specific spectral lines that were used to verify the solution. The following two columns give the redshift and uncertainty as obtained by fitting a model spectrum. The second to last column gives the best redshift which was obtained by shifting the model spectrum until it matched with spectral lines, or if a model spectrum was not used then it was obtained by matching specific spectral lines. The last column gives the perceived quality of the redshift on a scale of 1 - 3, where 1 is the lowest and 3 is the highest. Rows where the RA and DEC columns are empty should be interpreted as being the same as the above row, corresponding to cases where the same galaxy was observed through both slitmasks.

RA	DEC	Temp	Spectral Lines	z	σ_z	z (best)	Qual
02:15:54.03	-04:53:00.7	none	OII,CaK,CaH	none	none	0.945	1
02:15:54.52	-04:52:42.5	Early Spiral	OII,Hg,OIII	0.961	0.0010	0.959	3
		Early Spiral	OII,CaK,CaH,G	0.959	0.0007	0.959	3
02:15:50.64	-04:49:36.6	Elliptical	CaK,CaH,Hd	1.038	0.0007	1.038	3
		S0	CaK,CaH,Hd,G	1.038	0.0011	1.039	3
02:15:47.30	-04:49:18.2	Early Spiral	OII	1.150	0.0013	1.150	3
02:15:45.69	-04:49:46.0	Early Spiral	OII,CaK,CaH,Hd	1.004	0.0010	1.005	3
02:15:47.55	-04:50:15.1	Elliptical	CaK,CaH,Hd,G	0.954	0.0010	0.955	3
02:15:54.16	-04:51:08.2	none	none	none	none	none	1
02:15:54.98	-04:52:00.3	none	none	none	none	none	1
		Spiral	OII,CaK,CaH	1.167	0.0006	1.168	3
02:15:42.20	-04:52:19.9	none	none	none	none	none	1
		S0	CaK,CaH,G	0.954	0.0009	0.954	3
02:15:56.82	-04:51:26.2	Early Spiral	OII,CaK,CaH	1.024	0.0011	1.024	2
02:15:54.65	-04:50:46.0	Spiral	OII	1.025	0.0008	1.025	2
02:15:47.50	-04:50:04.0	none	none	none	none	none	1
		none	CaK,CaH,Hd,G	none	none	0.957	3
02:15:54.59	-04:49:55.0	S0	CaK,CaH,G	0.948	0.0014	0.949	2
02:15:52.07	-04:50:23.6	Elliptical	CaK,CaH,Hd,G	0.953	0.0012	0.954	3
02:15:54.00	-04:51:44.3	Elliptical	CaK,CaH,Hd,G	0.960	0.0011	0.959	3
		S0	CaK,CaH,Hd,G	0.957	0.0009	0.958	3
		S0	CaK,CaK,Hd,G	0.957	0.0010	0.958	3

Continued on next page...

Table 4.2 ...continued from previous page

RA	DEC	Temp	Spectral Lines	z	σ_z	z (best)	Qual
02:15:46.38	-04:50:36.7	Elliptical	CaK,CaH,G	0.935	0.0010	0.939	2
		S0	CaK,CaH,Hd,G	0.958	0.0014	0.956	3
02:15:51.54	-04:50:56.7	Elliptical	CaK,CaH,Hd,G	none	none	0.956	2
02:15:47.64	-04:50:10.8	Elliptical	CaK,CaH,G	0.946	0.0008	0.947	3
02:15:48.36	-04:49:33.3	Spiral	OII,H10	1.282	0.0007	1.282	3
		Spiral	OII,H10,H11	1.282	0.0006	1.283	3
02:15:50.96	-04:49:54.7	none	CaK,CaH,G	none	none	0.814	2
02:15:45.40	-04:49:40.4	Elliptical	CaK,CaH,Hd,G	0.954	0.0010	0.955	3
02:15:52.70	-04:48:29.3	none	none	none	none	none	1
02:15:48.02	-04:51:58.4	none	none	none	none	none	1
02:15:55.36	-04:50:34.6	S0	OII,CaK,CaH,Hd	1.023	0.0010	1.023	3
02:15:48.31	-04:52:19.6	none	none	none	none	none	1
02:15:45.40	-04:50:43.3	S0	CaK,CaH,Hd,G	0.955	0.0013	0.955	3
02:15:49.17	-04:50:38.6	Early Spiral	OII,CaK,CaH,Hd,G	0.898	0.0006	0.898	3
02:15:38.46	-04:51:51.5	Early Spiral	OII,CaK,CaH,Hd	1.099	0.0011	1.099	3
02:15:50.66	-04:53:11.4	Elliptical	CaK,CaH,Hd,G	0.752	0.0006	0.753	3
02:15:47.71	-04:50:21.2	none	OII,CaK,CaH	none	none	0.967	1
02:15:48.17	-04:50:30.5	Elliptical	CaK,CaH,Hd,G	0.963	0.0012	0.959	3
02:15:47.23	-04:50:14.2	Elliptical	CaK,CaH,G	0.947	0.0013	0.949	3
02:15:48.42	-04:50:18.9	Elliptical	CaK,CaH,G	0.953	0.0013	0.954	3
02:15:54.36	-04:48:29.1	none	none	none	none	none	1
02:15:45.65	-04:47:40.6	Spiral	OII,CaK,CaH,G	0.998	0.0016	1.002	2
02:15:53.47	-04:47:59.1	S0	OII,CaK,CaH,G	0.956	0.0018	0.957	3
02:15:56.35	-04:48:34.7	S0	OII,CaK,CaH,G	0.798	0.0010	0.798	3
02:15:51.36	-04:51:25.7	S0	CaK,CaH,Hd,G	0.959	0.0016	0.959	3
02:15:50.28	-04:52:14.3	Early Spiral	OII,Hg,OIII	1.002	0.0011	1.003	3
02:15:55.61	-04:50:31.2	Spiral	OII,CaK,CaH,Hd	1.052	0.0009	1.053	2
02:15:56.96	-04:50:39.3	S0	OII,CaK,CaH,G	0.877	0.0012	0.878	3
02:15:45.81	-04:53:06.9	S0	CaK,CaH,Hd,G	0.954	0.0008	0.956	3
02:15:58.28	-04:49:51.2	none	CaK,CaH,Hd,G	none	none	0.885	2
0.0	0.0	none	none	none	none	none	1
0.0	0.0	none	none	none	none	none	1
0.0	0.0	none	none	none	none	none	1
0.0	0.0	none	CaK,CaH,G	none	none	0.661	1
0.0	0.0	none	none	none	none	none	1
0.0	0.0	none	none	none	none	none	1
0.0	0.0	none	none	none	none	none	1
0.0	0.0	none	none	none	none	none	1
0.0	0.0	none	none	none	none	none	1
0.0	0.0	none	none	none	none	none	1
0.0	0.0	none	none	none	none	none	1
0.0	0.0	none	OII	none	none	0.943	1
0.0	0.0	Spiral	OII	0.716	0.0007	0.718	1
0.0	0.0	none	OII,G	none	none	0.670	1
0.0	0.0	Early Spiral	OII	0.653	0.0009	0.653	1
0.0	0.0	none	none	none	none	none	1
0.0	0.0	none	none	none	none	none	1
0.0	0.0	Elliptical	Hd,G	0.931	0.0020	0.931	1
0.0	0.0	S0	none	0.603	0.0010	none	1
0.0	0.0	none	none	none	none	none	1
0.0	0.0	none	none	none	none	none	1
0.0	0.0	none	none	none	none	none	1
0.0	0.0	none	none	none	none	none	1
0.0	0.0	none	none	none	none	none	1
0.0	0.0	Elliptical	OII	0.633	0.0024	0.628	1

Table 4.2: The redshift results for DES0215-0458. This table uses the same convention as Table 4.1.

In the results presented in Tables 4.1 & 4.2, there are some rows where the RA and DEC have the value of 0.0, these are all serendipitous galaxies that happened to be observed through the slits, but were not the intended targets of observation. Any trustworthy redshifts obtained from these will be used, but they are quite likely to be non-member galaxies. Fields in the table that have 'none' simply mean that nothing was used or obtained, depending on the context. For example, a very small number of the spectra had bad wavelength solutions, others had no discernable spectral features, others couldn't be fit with a model spectrum but had clearly visible features that were used to measure the redshift. Also, some of the serendipitous galaxies 'found' by the pipeline were on the edge of a slit making them either an artifact of the reduction process or having a signal-to-noise ratio that was too low. The ranking scheme of 1 - 3 was employed to distinguish trustworthy spectra from questionable or clearly erronious cases. A rating of 1 was used in any case where there was a bad wavelength solution, no spectral features, or it was clear that there was a problem during the data reduction. 2 was used when the fitted model had to be shifted substantially to line up, or when the fit looked reasonable but not dead on. Cases where the model fitting lined up tightly, or where only a very minor offset was needed to make the spectral features line up were given a rating of 3. As can be seen in the above tables, several galaxies where observed more than once due to the multiple slitmasks that were employed in observing each of the two clusters. In cases where trustworthy (quality = 3) redshifts are obtained, they agree very well. Additionally, in cases where one slit mask failed to provide a good observation of one galaxy, the other often did yield a good observation, and ultimately redshift.

To better visualize the distribution of trustworthy redshifts for each of the two DES clusters that were observed, the z (best) results were used to construct histograms. These histograms contain only the redshifts given a quality rating of 3, and cases where the same galaxy was observed more than once were treated by taking the mean of all measured redshifts for the galaxy thereby preventing any over-counting.

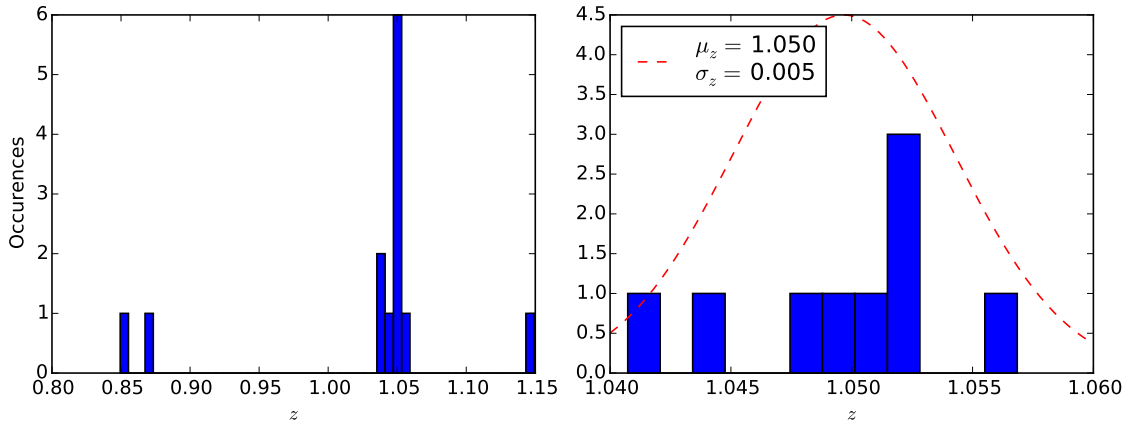

Figure 4.2: The left histogram contains all redshifts of the galaxies observed for DES0223-0416 that were given a quality rating of 3. The histogram on the right contains the subset of these galaxies that are suspected member-galaxies with a fitted Gaussian overlayed.

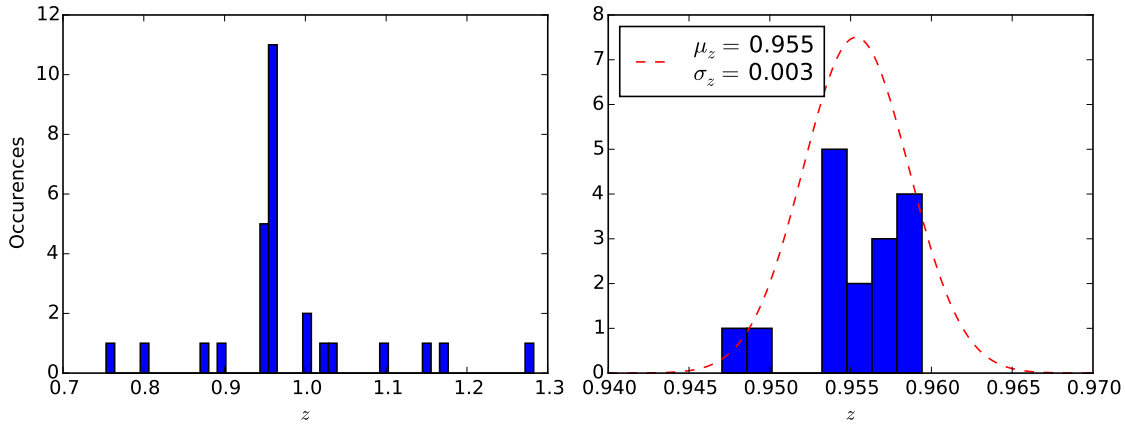

Figure 4.3: Histograms of the redshifts of the galaxies observed for DES0215-0458 following the same convention as in Figure 4.2.

The suspected member galaxies that are referenced in the right histograms from the above figures are simply those that were grouped tightly (from a visual inspection) about the highest bin in the left histogram for each figure. In the case of Figure 4.2 this range was $1.05 < z < 1.06$ and for Figure 4.3 it was $0.94 < z < 0.97$. The mean and standard deviation of the redshifts of the suspected member galaxies were taken for each cluster and then used to overplot the fitted Gaussians shown in the above figures, in this paper these means will be considered to be the central redshift of each cluster. The redshift of DES0223-0416 was

found to be 1.049 ± 0.005 and for DES0215-0458 it was found to be 0.955 ± 0.003.

4.2 Velocity Dispersion

After obtaining the redshift catalog given in Tables 4.1 & 4.2, the proper velocities, v_i, of the suspected member galaxies were obtained for each cluster using the following equation [11]:

$$v_i = \frac{z_i - z}{1 + z} c \tag{4.1}$$

Where z_i is the member galaxy redshift, z is the mean redshift for the cluster, and c is the speed of light.

After performing this calculation for each member galaxy in a cluster, the standard deviation was taken. This result is called the velocity dispersion, σ_r. Using this methodology, the velocity dispersion for DES0223-0416 was found to be 680 km s^{-1} and for DES0215-0458 it was found to be 510 km s^{-1}.

4.3 Cluster Mass

The mass of each cluster will be found using the following scaling relation [11]:

$$M \approx \left(\frac{\sigma_r}{939 z^{0.33}} \right)^{2.91} 10^{15} M_{\odot} \tag{4.2}$$

Performing this calculation for each cluster reveals that the mass of DES0223-0416 is approximately 3.7×10^{14} $M_{\odot}$ and that the mass of DES0215-0458 is approximately 1.7×10^{14} $M_{\odot}$.

5

Discussion

This paper presents high-resolution multi-slit spectroscopic observations made on two high redshift DES targeted galaxy clusters and the results obtained from them. The observations were collected over multiple nights using the DEIMOS instrument on Keck II at the W.M. Keck Observatory. The pre-existing Spec2d Data Reduction Pipeline was used, with modification, to reduce the raw data into science-ready one and two-dimensional spectra of the galaxies in each of the two observed clusters. The science-ready spectra were then analyzed with the aid of a tool called SpecPro to determine the redshifts of all of the observed galaxies.

For DES0223-0416, a total of 22 spectra were studied with SpecPro. Of these, a total of 13 unique[1], quality redshifts were obtained and of these 9 are from suspected member galaxies. In the case of DES0215-0458, a total of 76 spectra were studied. After averaging together multiple observations of the same galaxy and rejecting low quality spectra there are 28 unique, quality redshifts of which 16 are suspected to be member galaxies.

By taking the mean of all the redshifts of the suspected member galaxies, the redshift of DES0223-0416 was found to be 1.049 ± 0.005 and the redshift of DES0215-0458 to be 0.955 ± 0.003. Using these results the velocity dispersion for DES0223-0416 was determined to be 680 km s^{-1} and for DES0215-0458 it was found to be 510 km s^{-1}. Finally, the masses of

[1]This counts galaxies observed through both slitmasks only once

DES0223-0416 and DES0215-0458 were calculated to be $3.7 \times 10^{14}\ M_{\odot}$ and $1.7 \times 10^{14}\ M_{\odot}$, respectively. The catalog of redshifts and the results obtained from it will be added to catalogs of lower redshift clusters produced by other DES groups, ultimately leading to a robust sample of redshifts that DES will use to constrain and calibrate their results.

Appendix A

Spec2d Modifications

The beta version of the Spec2d Data Reduction Pipeline was modified as follows:
In the `deimos_mask_calibrate.pro` routine after the call to `deimos_omodel` (around line 300) the following code was added (the call to `deimos_omodel` is also shown for reference):

```
; process optical model for this chip
   model_lambda =  deimos_omodel(chipno, slitcoords, arc_header)


   nloop = n_elements(model_lambda)
   for ii=0,nloop-1 do begin
       if model_lambda[ii].lambda_y[0] gt 0 then begin
           model_lambda[ii].lambda_y[0] = model_lambda[ii].lambda_y[0] + 50.
           model_lambda[ii].lambda_y_top[0] = model_lambda[ii].lambda_y_top[0] + 50.
           model_lambda[ii].lambda_y_bottom[0] = model_lambda[ii].lambda_y_bottom[0] + 50.
       endif
   endfor
   nslits=total(model_lambda.xb gt 0 AND model_lambda.xt gt 0)
```

In essence, this alteration just moves the optical model guess for the wavelength solution by 50 angstroms (in this case, though other guesses aside from 50 could be used).

Appendix B

Sample Plan File

The plan file (`0223_2.plan`) used to reduce mask '0223_2' is shown below. Note that the first two lines are note interpreted by `domask.pro` because of the escape character (#).

```
# Plan file auto-generated by deimos_planfile.pro Wed Apr 22 15:01:01 2015
# Grating: 1200G       Grangle:       10.1388
MASK: 0223_2
RAWDATADIR: /DES_work/keck_obs/2014sep21/raw
CHIPS: 2,3,6,7
polyflag   - use polyflag for fitting lambda
FLATNAME: d0921_0017.fits
FLATNAME: d0921_0018.fits
FLATNAME: d0921_0019.fits
FLATNAME: d0921_0020.fits
FLATNAME: d0921_0021.fits
FLATNAME: d0921_0022.fits
FLATNAME: d0921_0023.fits
FLATNAME: d0921_0024.fits
FLATNAME: d0921_0025.fits
FLATNAME: d0921_0026.fits
ARCNAME: d0921_0015.fits
ARCNAME: d0921_0016.fits
SCIENCENAME: d0921_0029.fits
SCIENCENAME: d0921_0030.fits
SCIENCENAME: d0921_0032.fits
SCIENCENAME: d0921_0033.fits
SCIENCENAME: d0921_0035.fits
SCIENCENAME: d0921_0036.fits
```

Bibliography

[1] *Keck DEIMOS 1D/2D wrapper*. Available: `http://specpro.caltech.edu/specpro_wrappers.html`.

[2] S. Carroll. The Cosmological Constant. *Living Rev. Relativity*, 4, 2001.

[3] M. C. Cooper, J. A. Newman, M. Davis, D. P. Finkbeiner, and B. F. Gerke. spec2d: DEEP2 DEIMOS Spectral Pipeline. Astrophysics Source Code Library, March 2012.

[4] Edwin Hubble. A Relation Between Distance and Radial Velocity Among Extra-Galactic Nebulae. *Proceedings of the National Academy of Sciences*, 15(3):168–173, 1929.

[5] R. Kallosh and A. Linde. Dark Energy and the Fate of the Universe. *JCA*, 2:2, Feb 2003.

[6] D. Masters and P. Capak. SpecPro: An Interactive IDL Program for Viewing and Analyzing Astronomical Spectra. *PASP*, 123:638–644, May 2011.

[7] J. A. Newman, M. C. Cooper, M. Davis, S. M. Faber, A. L. Coil, P. Guhathakurta, D. C. Koo, A. C. Phillips, C. Conroy, A. A. Dutton, D. P. Finkbeiner, B. F. Gerke, D. J. Rosario, B. J. Weiner, C. N. A. Willmer, R. Yan, J. J. Harker, S. A. Kassin, N. P. Konidaris, K. Lai, D. S. Madgwick, K. G. Noeske, G. D. Wirth, A. J. Connolly, N. Kaiser, E. N. Kirby, B. C. Lemaux, L. Lin, J. M. Lotz, G. A. Luppino, C. Marinoni, D. J. Matthews, A. Metevier, and R. P. Schiavon. The DEEP2 Galaxy Redshift Survey: Design, Observations, Data Reduction, and Redshifts. *ApJS*, 208:5, September 2013.

[8] S. Perlmutter, G. Aldering, G. Goldhaber, R. A. Knop, P. Nugent, P. G. Castro, S. Deustua, S. Fabbro, A. Goobar, D. E. Groom, I. M. Hook, A. G. Kim, M. Y. Kim, J. C. Lee, N. J. Nunes, R. Pain, C. R. Pennypacker, R. Quimby, C. Lidman, R. S. Ellis, M. Irwin, R. G. McMahon, P. Ruiz-Lapuente, N. Walton, B. Schaefer, B. J. Boyle, A. V. Filippenko, T. Matheson, A. S. Fruchter, N. Panagia, H. J. M. Newberg, W. J. Couch, and T. S. C. Project. Measurements of Ω and Λ from 42 High-Redshift Supernovae. *ApJ*, 517:565–586, June 1999.

[9] Planck Collaboration, P. A. R. Ade, N. Aghanim, M. I. R. Alves, C. Armitage-Caplan, M. Arnaud, M. Ashdown, F. Atrio-Barandela, J. Aumont, H. Aussel, and et al. Planck 2013 results. I. Overview of products and scientific results. *AAP*, 571:A1, November 2014.

[10] A. G. Riess, A. V. Filippenko, P. Challis, A. Clocchiatti, A. Diercks, P. M. Garnavich, R. L. Gilliland, C. J. Hogan, S. Jha, R. P. Kirshner, B. Leibundgut, M. M. Phillips, D. Reiss, B. P. Schmidt, R. A. Schommer, R. C. Smith, J. Spyromilio, C. Stubbs, N. B. Suntzeff, and J. Tonry. Observational Evidence from Supernovae for an Accelerating Universe and a Cosmological Constant. *AJ*, 116:1009–1038, September 1998.

[11] J. Ruel, G. Bazin, M. Bayliss, M. Brodwin, R. J. Foley, B. Stalder, K. A. Aird, R. Armstrong, M. L. N. Ashby, M. Bautz, B. A. Benson, L. E. Bleem, S. Bocquet, J. E. Carlstrom, C. L. Chang, S. C. Chapman, H. M. Cho, A. Clocchiatti, T. M. Crawford, A. T. Crites, T. de Haan, S. Desai, M. A. Dobbs, J. P. Dudley, W. R. Forman, E. M. George, M. D. Gladders, A. H. Gonzalez, N. W. Halverson, N. L. Harrington, F. W. High, G. P. Holder, W. L. Holzapfel, J. D. Hrubes, C. Jones, M. Joy, R. Keisler, L. Knox, A. T. Lee, E. M. Leitch, J. Liu, M. Lueker, D. Luong-Van, A. Mantz, D. P. Marrone, M. McDonald, J. J. McMahon, J. Mehl, S. S. Meyer, L. Mocanu, J. J. Mohr, T. E. Montroy, S. S. Murray, T. Natoli, D. Nurgaliev, S. Padin, T. Plagge, C. Pryke, C. L. Reichardt, A. Rest, J. E. Ruhl, B. R. Saliwanchik, A. Saro, J. T. Sayre, K. K. Schaffer, L. Shaw, E. Shirokoff, J. Song, R. Šuhada, H. G. Spieler, S. A. Stanford,

Z. Staniszewski, A. A. Starsk, K. Story, C. W. Stubbs, A. van Engelen, K. Vanderlinde, J. D. Vieira, A. Vikhlinin, R. Williamson, O. Zahn, and A. Zenteno. Optical Spectroscopy and Velocity Dispersions of Galaxy Clusters from the SPT-SZ Survey. *ApjJ*, 792:45, September 2014.

[12] E Sánchez and the DES Collaboration. The Dark Energy Survey. *Journal of Physics: Conference Series*, 259(1):012080, 2010.

[13] UC Irvine. *DEEP2 Spec2d Cookbook*. Available: `http://deep.ps.uci.edu/spec2d/cookbook.html`.

[14] W.M. Keck Observatory, Mauna Kea, Hawaii. *DEIMOS Afternoon Checklist*. Available: `http://www2.keck.hawaii.edu/inst/deimos/checklist-pm.html`.

[15] W.M. Keck Observatory, Mauna Kea, Hawaii. *DEIMOS Home Page*. Available: `http://www2.keck.hawaii.edu/inst/deimos/`.